



## Original article

Iron(III) oxide-hydroxide modification on *Pterocarpus macrocarpus* sawdust beads for direct red 28 dye removalPornsawai Praipipat<sup>a,b,\*</sup>, Pimploj Ngamsurach<sup>a,b</sup>, Piyaporn Khamkhae<sup>a</sup><sup>a</sup> Department of Environmental Science, Khon Kaen University, Khon Kaen 40002, Thailand<sup>b</sup> Environmental Applications of Recycled and Natural Materials (EARN) Laboratory, Khon Kaen University, Khon Kaen 40002, Thailand

## ARTICLE INFO

## Keywords:

Industrial waste  
Iron(III) oxide-hydroxide  
Adsorption  
Anionic dye  
Reusability

## ABSTRACT

The releasing of wastewater contaminated with direct red 28 (DR28) dye into receiving water is a concern because it is a polyaromatic structure with difficult biodegradation. It results in being persistent in the environment and being toxic to the ecosystem from accumulating through a food chain. Thus, it needs to eliminate DR28 dye from contaminated wastewater. Sawdust beads (SDB) and sawdust mixed with iron(III) oxide-hydroxide beads (SDFB) are prepared and characterized for DR28 dye removals. DR28 dye removal efficiencies are examined with various affecting factors by the batch tests and adsorption-desorption tests, and their adsorption patterns, rates, and mechanisms are determined by isotherms and kinetics models. Moreover, the thermodynamic studies are examined for the temperature effect. SDFB demonstrated a higher surface area and smaller pore size than SDB. SDB and SDFB were uneven shapes and heterogeneous fibrillar structures. Carbon, oxygen, calcium, chloride, sodium, O—H, C—H, C=C, —COOH, and C—O were found in SDB and SDFB. The points of zero charge of SDB and SDFB were 4.65 and 6.11. The conditions of 3.5 g, 50 °C, pH 3, 60 mg/L and 2.5 g, 40 °C, pH 3, 60 mg/L illustrated the highest DR28 dye removals of more than 82 % for SDB and SDFB, respectively. Thus, the material modification by iron(III) oxide-hydroxide improved the DR28 dye removal efficiency of sawdust material. Moreover, they could be reusability more than three times with DR28 dye removal of more than 63 %. SDB and SDFB corresponded to Langmuir and Freundlich models, respectively, and a pseudo-second-order was a good model to describe their adsorption mechanism. Both materials did not favor DR28 dye adsorptions with increasing temperature. Therefore, SDFB was a potential material for removing DR28 dye removal in the industrial wastewater.

## 1. Introduction

Increasing dye uses in the industrial production processes from pigment, dye, textile, leather, plastic, food, pharmaceutical, paint, and paper factories result in a high risk of dye-contaminated wastewater and affecting the environment because they are polyaromatic structures, toxicity to the ecosystem, bioaccumulation through the food web, and difficult biodegradation (Islam et al., 2023). Several anionic dyes of reactive, acid, azo, and direct are used in the above industries with different purposes. Since direct dyes are easy to use with long-lasting dyes and are cheaper price than other dye types, they are popularly used for dyeing lignin cellulose, and cotton, especially direct red 28 (DR28) dye. It is commonly used by several manufacturers of textile, printing, and paper (Benkhaya et al., 2020). Since the structure of DR28 dye includes two azo groups which are tetrazotized benzidine and

naphthionic acid, it is difficult to degrade and be persistent in the environment for a long time (Siddiqui et al., 2023). In addition, the release of wastewater contaminated DR28 dye into water bodies blocks the photosynthesis of aquatic organisms and decreases dissolved oxygen in water affecting the water quality and aquatic life (Tkaczyk et al., 2020). Moreover, its toxicity also causes human carcinogens and anaphylactic shock (Oladoye et al., 2022). Therefore, the wastewater contaminated with DR28 dye needs to be treated before being released to the water bodies to protect the aquatic life and environment.

Several chemical or physiochemical methods such as coagulation-flocculation, precipitation, adsorption, chemical oxidation, electrochemistry, photochemical, reverse osmosis, and membrane filtration used to eliminate wastewater-contaminated dyes. Among those methods, adsorption is a good option because it offers an effective method, reasonable cost, adsorbent reusability, and various availability

\* Corresponding author at: Department of Environmental Science, Khon Kaen University, Khon Kaen 40002, Thailand.

E-mail address: [pornprai@kku.ac.th](mailto:pornprai@kku.ac.th) (P. Praipipat).<https://doi.org/10.1016/j.arabjc.2023.105514>

Received 7 October 2023; Accepted 30 November 2023

Available online 2 December 2023

1878-5352/© 2023 The Author(s). Published by Elsevier B.V. on behalf of King Saud University. This is an open access article under the CC BY-NC-ND license (<http://creativecommons.org/licenses/by-nc-nd/4.0/>).

of adsorbent choices (Dutta et al., 2021). Commercial adsorbents, biosorbents, nanosorbents, and waste adsorbents are used to remove various dyes shown in Table 1. For commercial adsorbents, activated carbon, and chitosan have been used for acid yellow 23 and methylene blue (MB) dye adsorptions (Ahmad and Ansari, 2021; Khader et al., 2021). *Pinus roxburghii* leaves, *Dodonaea viscosa* bark, and apple leaves activated carbon are used to adsorb acid orange 74, methyl red, and basic blue 47 dyes as biosorbents (Abdel-Aziz et al., 2021; Gul et al., 2022; Rehman et al., 2019). For nanosorbents, MB dye is adsorbed by wheat straw modified with magnetic nanoparticles (Ebrahimian Pirbazarzi et al., 2014). For food waste adsorbents, lemon peel, chicken and duck eggshells, coffee waste modified with polyethylenimine, and almond shell are used to remove eosin, reactive blue 4 (RB4), reactive black 5, and crystal violet dyes (Bukhari et al., 2022; Loulidi et al., 2020; Praipipat et al., 2022b; Wong et al., 2020). Basic red 2 and RB4 dyes are adsorbed by agriculture waste adsorbents of sugarcane bagasse (Farahani et al., 2015; Praipipat et al., 2023h). For industrial waste adsorbents, sugarcane bagasse fly ash and sawdust are used for adsorbing DR28, RB4, MB, methyl violet (MV), and crystal violet dyes (Ahmad and Nasar, 2023; Esmaeili and Foroutan, 2019; Guechi et al., 2021; Muneer et al., 2021; Praipipat et al., 2023b, 2023d, 2023b). For DR28 dye adsorption, various adsorbent types above have been used to eliminate it. Zeolite A and chitosan are used as commercial adsorbents

(Ahmad and Ansari, 2021; Khalaf et al., 2021), and calcinated kaolin is used as a biosorbent (Findik, 2023). The cotton stalks biochar modified with zinc oxide nanocomposite and carbon nanotube mixed metal oxides nanocomposites are used as nanosorbents (Iqbal et al., 2021; Yang et al., 2015). Moreover, banana peel, cabbage, coffee, rice husk, sugarcane bagasse, sugarcane bagasse fly ash, pine bark, and sawdust have been used for removing DR28 dye in many previous studies, and the details are demonstrated in Table 1. Among the adsorbents mentioned above, the waste adsorbents are interesting because only uses of waste adsorbents could reduce waste volumes for waste management but also they can improve wastewater quality by adsorbing several dyes. Especially, sawdust is a good selection because it has a high adsorption capacity among other adsorbents in Table 1. It consists of cellulose, hemicellulose, and lignin, and then it can adsorb dyes in wastewater. However, the modification of sawdust needs more investigations to deal with the high dye concentrations in real wastewater.

Since increasing the adsorbent capacity is needed to deal with a high dye concentration in wastewater, metal oxide is popularly used to modify adsorbent. It increases the specific surface area of adsorbent resulting in capable high dye removal. Iron(II or III) oxide, magnesium oxide (MgO), aluminum oxide (Al<sub>2</sub>O<sub>3</sub>), zinc oxide (ZnO), iron(III) oxide-hydroxide, and titanium dioxide (TiO<sub>2</sub>) are used in previous studies to encourage dye removal efficiency shown in Table 2. Iron(II or III) oxide

**Table 1**  
Several adsorbents for dye removals in aqueous solution.

Materials	Dyes	Types	q <sub>m</sub> (mg/g)	References
<b>Commercials</b>				
Activated carbon	Acid yellow 23	Anionic	10.20	(Khader et al., 2021)
Zeolite A	Direct red 28	Anionic	21.11	(Khalaf et al., 2021)
Chitosan	Direct red 28	Anionic	104.60	(Ahmad and Ansari, 2021)
Chitosan	Methylene blue	Cationic	99.01	(Ahmad and Ansari, 2021)
<b>Biosorbents</b>				
Calcined kaolin	Direct red 28	Anionic	5.39	(Findik, 2023)
<i>Pinus roxburghii</i> leaves	Acid orange 74	Anionic	7.52	(Rehman et al., 2019)
<i>Dodonaea viscosa</i> bark	Methyl red	Anionic	2.54	(Gul et al., 2022)
Apple leaves activated carbon	Basic blue 47	Cationic	2.59	(Abdel-Aziz et al., 2021)
<b>Nanosorbents</b>				
Cotton stalks biochar modified with zinc oxide nanocomposite	Direct red 28	Anionic	555.60	(Iqbal et al., 2021)
Carbon nanotube mixed metal oxides nanocomposites	Direct red 28	Anionic	1250.00	(Yang et al., 2015)
Wheat straw modified with magnetic nanoparticles	Methylene blue	Cationic	1374.60	(Ebrahimian Pirbazarzi et al., 2014)
<b>Waste adsorbents</b>				
<b>Food wastes</b>				
Banana peel	Direct red 28	Anionic	1.72	(Mondal and Kar, 2018)
Cabbage	Direct red 28	Anionic	2.31	(Wekoye et al., 2020)
Lemon peel	Eosin	Anionic	8.24	(Bukhari et al., 2022)
Chicken eggshell beads	Reactive blue 4	Anionic	24.10	(Praipipat et al., 2022b)
Duck eggshell beads	Reactive blue 4	Anionic	12.63	(Praipipat et al., 2022b)
Coffee waste modified with polyethylenimine	Reactive black 5	Anionic	77.52	(Wong et al., 2020)
Coffee waste modified with polyethylenimine	Direct red 28	Anionic	34.36	(Wong et al., 2020)
Almond shell	Crystal violet	Cationic	12.20	(Loulidi et al., 2020)
<b>Agriculture wastes</b>				
Rice husk char	Direct red 28	Anionic	1.28	(Malik et al., 2020)
Rice husk	Direct red 28	Anionic	1.58	(Malik et al., 2020)
Rice husk char modified potassium hydroxide	Direct red 28	Anionic	2.04	(Malik et al., 2020)
Sugarcane bagasse	Basic red 2	Cationic	58.85	(Farahani et al., 2015)
Bagasse beads	Reactive blue 4	Anionic	2.77	(Praipipat et al., 2023h)
Sugarcane bagasse beads	Direct red 28	Anionic	3.24	(Patabandige et al., 2019)
Rice husk modified with phosphoric acid	Reactive black 5	Anionic	2.60	(Değermenci et al., 2019)
Corn silk	Reactive blue 19	Anionic	60.60	(Değermenci et al., 2019)
Corn silk	Reactive red 218	Anionic	51.60	(Farahani et al., 2015)
<b>Industrial wastes</b>				
Bagasse fly ash beads	Reactive blue 4	Anionic	2.72	(Praipipat et al., 2023h)
Sawdust beads	Reactive blue 4	Anionic	7.61	(Praipipat et al., 2023b)
Pine bark	Direct red 28	Anionic	3.92	(Litefti et al., 2019)
Fly ash	Direct red 28	Anionic	22.12	(Harja et al., 2022)
Sugarcane bagasse fly ash beads	Direct red 28	Anionic	3.36	(Praipipat et al., 2023d)
<i>Cedrus deodara</i> sawdust	Direct red 28	Anionic	182.50	(Muneer et al., 2021)
Palm sawdust	Methylene blue	Cationic	53.95	(Esmaeili and Foroutan, 2019)
Eucalyptus sawdust	Methylene blue	Cationic	53.48	(Esmaeili and Foroutan, 2019)
Sour lemon sawdust	Methylene blue	Cationic	52.36	(Esmaeili and Foroutan, 2019)
Okoume sawdust	Methyl violet 2B	Cationic	102.04	(Guechi et al., 2021)
<i>Azadirachta indica</i> sawdust	Crystal violet	Cationic	270.27	(Ahmad and Nasar, 2023)

is used to modify clay and wheat bran sawdust to remove alizarin red s, MB, and MV dyes (Fu et al., 2011; Pooladi et al., 2021). Lemon peel, chicken or duck eggshells, bagasse or bagasse fly ash, chitosan, activated carbon oak wood, and sawdust are modified by ZnO to adsorb RB4, DR28, malachite green, methyl violet 2B, and MB dyes (Foroutan et al., 2022; Muinde et al., 2020; Ngamsurach et al., 2022; Oyewo et al., 2020; Praipipat et al., 2022a, 2022b, 2023d). TiO<sub>2</sub>, Al<sub>2</sub>O<sub>3</sub>, and MgO are used for modifying bagasse or bagasse fly ash for RB4 and DR28 dye adsorptions (Praipipat et al., 2023h, 2023d). Since many previous studies affirmed the high capability of iron(III) oxide-hydroxide modified with various waste adsorbents for dye adsorptions shown in Table 2, it is a good choice of metal oxide for the raw material modification to improve its ability to remove target pollutants. Although iron(III) oxide-hydroxide has been applied for modifying raw materials of lemon peels, eggshells, bagasse, bagasse fly ash, and sawdust to adsorb RB4 dye, DR28 dye removal by those adsorbents has not yet been investigated. Therefore, this study is the first attempt to use sawdust modified iron(III) oxide-hydroxide to eliminate DR28 dye.

The current study aimed to synthesize sawdust beads (SDB) and sawdust mixed with iron(III) oxide-hydroxide beads (SDFB) to adsorb DR28 dye with various material characterizations on the physicochemical properties, surface structure, chemical elements, and chemical functional groups including the point of zero charge. DR28 dye removal efficiencies are examined through batch tests, adsorption-desorption tests, adsorption isotherms, adsorption kinetics, and thermodynamic studies.

## 2. Materials and methods

### 2.1. Raw material

Sawdust (*Pterocarpus indicus*) was collected from a sawmill in Udon Thani province, Thailand.

**Table 2**

Various metal oxide modifications in waste adsorptions for anionic and cationic dye adsorptions.

Modifications/Raw materials	Dyes	Types	q <sub>m</sub> (mg/g)	References
<b>Zinc oxide (ZnO)</b>				
Lemon peel	Reactive blue 4	Anionic	2.59	(Praipipat et al., 2022a)
Chicken eggshell	Reactive blue 4	Anionic	20.41	(Praipipat et al., 2022b)
Duck eggshell	Reactive blue 4	Anionic	19.23	(Praipipat et al., 2022b)
Bagasse	Reactive blue 4	Anionic	3.18	(Ngamsurach et al., 2022)
Bagasse fly ash	Reactive blue 4	Anionic	6.78	(Praipipat et al., 2022b)
Sugarcane bagasse fly ash	Direct red 28	Anionic	3.90	(Praipipat et al., 2023d)
Chitosan	Malachite green	Cationic	11.00	(Muinde et al., 2020)
Activated carbon oak wood	Methyl violet 2B	Cationic	37.05	(Foroutan et al., 2022)
Sawdust	Methylene blue	Cationic	64.93	(Oyewo et al., 2020)
<b>Titanium dioxide (TiO<sub>2</sub>)</b>				
Bagasse	Reactive blue 4	Anionic	5.55	(Praipipat et al., 2023h)
Bagasse fly ash	Reactive blue 4	Anionic	6.48	(Praipipat et al., 2023h)
Sugarcane bagasse fly ash	Direct red 28	Anionic	4.00	(Praipipat et al., 2023d)
<b>Aluminum oxide (Al<sub>2</sub>O<sub>3</sub>)</b>				
Bagasse	Reactive blue 4	Anionic	3.41	(Praipipat et al., 2023h)
Bagasse fly ash	Reactive blue 4	Anionic	5.11	(Praipipat et al., 2023h)
Sugarcane bagasse fly ash	Direct red 28	Anionic	5.46	(Praipipat et al., 2023d)
<b>Magnesium oxide (MgO)</b>				
Bagasse	Reactive blue 4	Anionic	5.55	(Praipipat et al., 2023h)
Bagasse fly ash	Reactive blue 4	Anionic	6.48	(Praipipat et al., 2023h)
Sugarcane bagasse fly ash	Direct red 28	Anionic	5.56	(Praipipat et al., 2023d)
<b>Iron(II or III) oxide (Fe<sub>3</sub>O<sub>4</sub>)</b>				
Clay	Alizarin red s	Anionic	32.70	(Fu et al., 2011)
Wheat bran sawdust	Methylene blue	Cationic	51.28	(Pooladi et al., 2021)
Wheat bran sawdust	Methyl violet	Cationic	46.08	(Pooladi et al., 2021)
<b>Iron(III) oxide-hydroxide</b>				
Lemon peel	Reactive blue 4	Anionic	3.23	(Praipipat et al., 2022a)
Chicken eggshell	Reactive blue 4	Anionic	30.49	(Praipipat et al., 2022b)
Duck eggshell	Reactive blue 4	Anionic	25.97	(Praipipat et al., 2022b)
Bagasse	Reactive blue 4	Anionic	3.77	(Praipipat et al., 2022b)
Bagasse fly ash	Reactive blue 4	Anionic	10.28	(Praipipat et al., 2022b)
Sawdust	Reactive blue 4	Anionic	10.31	(Praipipat et al., 2023b)

### 2.2. Chemicals

All chemicals were analytical grades (AR) used without purification which were ferric chloride hexahydrate (FeCl<sub>3</sub>·6H<sub>2</sub>O) (LOBA, India), sodium hydroxide (NaOH) (RCI Labscan, Thailand), sodium alginate (NaC<sub>6</sub>H<sub>7</sub>O<sub>6</sub>) (Merck, Germany), and calcium chloride dehydrate (CaCl<sub>2</sub>·2H<sub>2</sub>O) (RCI Labscan, Thailand), and DR28 dye (C<sub>32</sub>H<sub>22</sub>N<sub>6</sub>O<sub>6</sub>S<sub>2</sub>Na<sub>2</sub>) (Merk, Germany). For a pH adjustment, 0.1 M NaOH and 0.1 M hydrochloric acid (HCl) (RCI Labscan, Thailand) were used.

### 2.3. Sawdust material synthesis

The synthesis methods of SDB and SDFB explained by the schematic flow diagram are demonstrated in Fig. 1a and b which referred to the study of Praipipat et al. (Praipipat et al., 2023b).

### 2.4. Material characterizations

Brunauer-Emmett-Teller (BET) (Bel, Bel Sorp mini X, Japan) is used to determine the physicochemical properties of SDB and SDFB, and their surface morphologies and chemical elements are explored by Field Emission Scanning Electron Microscopy and Focus Ion Beam (FESEM-FIB) with Energy Dispersive X-Ray Spectrometer (EDX) (FEI, Helios NanoLab G3 CX, USA). The chemical functional groups are identified by Fourier Transform Infrared Spectroscopy (FT-IR) (Bruker, TENSOR27, Hong Kong).

### 2.5. The point of zero charge

The surface charge of the adsorbent is necessary to investigate and predict how the adsorption occurs when the anionic pollutant might be adsorbed by a positively charged adsorbent. On the opposite, the

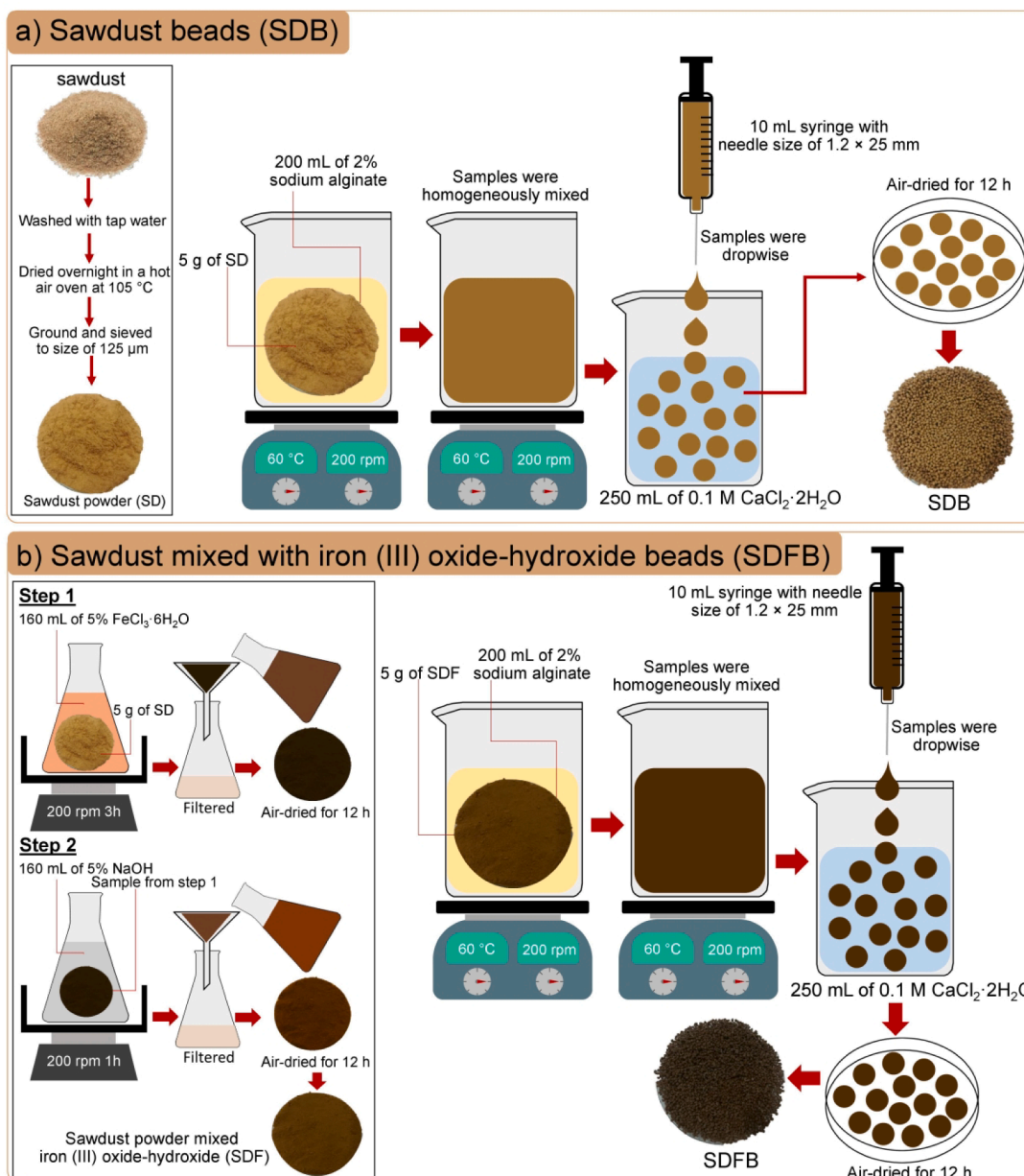


Fig. 1. The synthesis methods of (a) SDB and (b) SDFB in the schematic flow diagram.

Table 3  
Isotherm model equations.

Models	Full equations	Plotting graph	Eq	References
<b>Linear</b>				
Langmuir	$\frac{C_e}{q_e} = \frac{1}{q_m K_L} + \frac{C_e}{q_m}$	$\frac{C_e}{q_e}$ versus $C_e$	(3)	(Langmuir, 1918)
Freundlich	$\log q_e = \log K_F + \frac{1}{n} \log C_e$	$\log q_e$ versus $\log C_e$	(4)	(Freundlich, 1906)
Temkin	$q_e = \frac{RT}{b_T} \ln A_T + \frac{RT}{b_T} \ln C_e$	$q_e$ versus $\ln C_e$	(5)	(Temkin and Pyzhev, 1940)
Dubinin-Radushkevich	$\ln q_e = \ln q_m - K_{DR} \epsilon^2$	$\ln q_e$ versus $\epsilon^2$	(6)	(Dubinin and Radushkevich, 1947)
<b>Nonlinear</b>				
Langmuir	$q_e = \frac{q_m K_L C_e}{1 + K_L C_e}$	$q_e$ versus $C_e$	(7)	(Langmuir, 1918)
Freundlich	$q_e = K_F C_e^{1/n}$	$q_e$ versus $C_e$	(8)	(Freundlich, 1906)
Temkin	$q_e = \frac{RT}{b_T} \ln A_T C_e$	$q_e$ versus $C_e$	(9)	(Temkin and Pyzhev, 1940)
Dubinin-Radushkevich	$q_e = q_m \exp(-K_{DR} \epsilon^2)$	$q_e$ versus $C_e$	(10)	(Dubinin and Radushkevich, 1947)

**Table 4**  
Kinetic model equations.

Models	Full equations	Plotting graph	Eq	References
<b>Linear</b>				
Pseudo-first-order	$\ln(q_e - q_t) = \ln q_e - k_1 t$	$\ln(q_e - q_t)$ versus time (t)	(11)	(Lagergren, 1898)
Pseudo-second-order	$\frac{t}{q_t} = \frac{1}{k_2 q_e^2} + \left(\frac{1}{q_e}\right)t$	$\frac{t}{q_t}$ versus time (t)	(12)	(Ho and McKay, 1999)
Elovich	$q_t = \frac{1}{\beta} \ln(\alpha\beta) + \frac{1}{\beta} \ln t$	$q_t$ versus $\ln t$	(13)	(Elovich and Larinov, 1962)
Intraparticle diffusion	$q_t = k_i t^{0.5} + C_i$	$q_t$ versus time (t <sup>0.5</sup> )	(14)	(Weber and Morris, 1963)
<b>Nonlinear</b>				
Pseudo-first-order	$q_t = q_e (1 - e^{-k_1 t})$	$q_t$ versus time (t)	(15)	(Lagergren, 1898)
Pseudo-second-order	$q_t = \frac{k_2 q_e^2 t}{1 + q_e k_2 t}$	$q_t$ versus time (t)	(16)	(Ho and McKay, 1999)
Elovich	$q_t = \beta \ln t + \beta \ln \alpha$	$q_t$ versus time (t)	(17)	(Elovich and Larinov, 1962)
Intraparticle diffusion	$q_t = k_i t^{0.5} + C_i$	$q_t$ versus time (t)	(18)	(Weber and Morris, 1963)

**Fig. 2.** The physical characteristics of (a) SDB and (b) SDFB.**Table 5**

The physiochemical properties of SDB and SDFB.

	SDB	SDFB
BET specific surface area (m <sup>2</sup> /g)	1.138	12.540
Pore volume (cm <sup>3</sup> /g)	0.301	2.714
Pore diameter size (nm)	4.634	4.306

cationic pollutant might be adsorbed by a negatively charged adsorbent. Thus, the points of zero charge (pH<sub>pzc</sub>) of SDB and SDFB for removing DR28 dye are required to explore this curiosity above which this study used the method of Praipipat et al. (Praipipat et al., 2023f). Firstly, 0.1 M NaCl solutions were prepared in pH 1–12, and 50 mL of each pH solution was contained in a 250 mL Erlenmeyer flask. Then, 0.1 g of SDB or SDFB were added and shaken by an orbital shaker (GFL, 3020, Germany) at 150 rpm for 24 h. The pH<sub>pzc</sub> was calculated from the plotting graph of ΔpH (pH<sub>final</sub> – pH<sub>initial</sub>) versus pH<sub>initial</sub> which a pH value was measured by a pH meter (Mettler Toledo, SevenGo with InLab 413/IP67, Switzerland).

## 2.6. Batch tests

Batch tests are investigated to explore the effects of dosage from 2 to 4 g, temperature from 30 to 70 °C, pH 1–11, and concentration from 40 to 80 mg/L with a DR28 dye concentration of 60 mg/L, 200 mL of sample volume, 12 h, and 150 rpm of shaking speed for DR28 dye removals by SDB and SDFB. The lowest value of each affecting factor offering the highest DR28 dye removal efficiency is selected for the optimum condition (Praipipat et al., 2023b). The results were confirmed with the triplicate experiments and the average result was reported. The dye concentration was measured by UV–VIS Spectrophotometer (Hitachi, UH5300, Japan), and Equation (1) was used to calculate dye removal efficiency in the percentage (%).

$$\text{Dye removal efficiency (\%)} = \left( \frac{C_0 - C_e}{C_0} \right) \times 100 \quad (1)$$

where C<sub>0</sub> is the initial dye concentration (mg/L), and C<sub>e</sub> is the final dye concentration (mg/L).

## 2.7. The adsorption–desorption tests

The reusability of materials is a necessary investigation before applying them in the industry to evaluate the cost-effectiveness of the material in use. This study used the method of Praipipat et al. (Praipipat et al., 2023b) for investigating adsorption–desorption tests of SDB and SDFB for removing DR28 dye in three cycles. After DR28 dye adsorption, the saturated SDB or SDFB was added to 250 mL of Erlenmeyer flask containing 200 mL of 0.01 M NaOH solution, then it was shaken by an

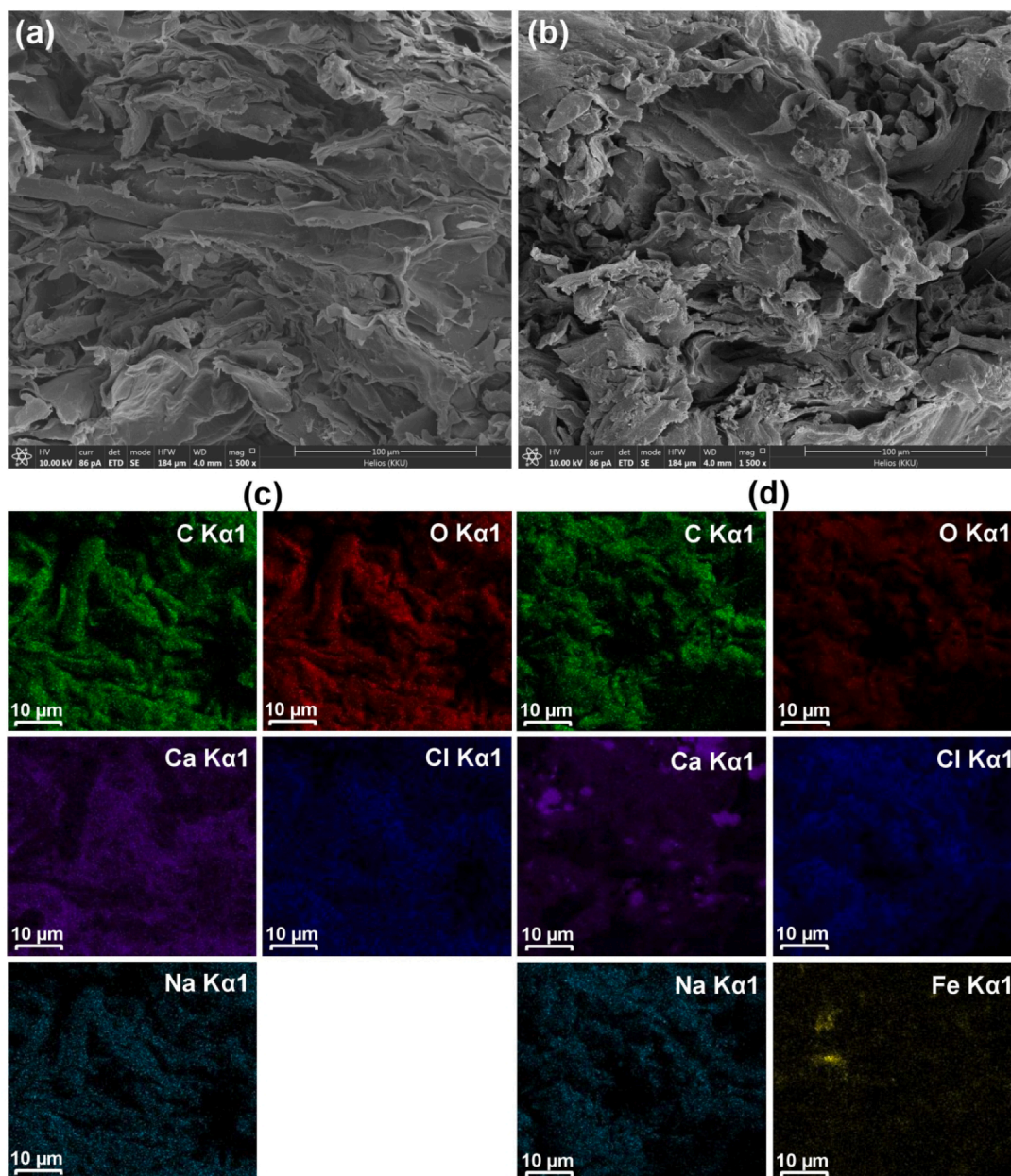


Fig. 3. The surface morphologies of (a) SDB, (b) SDFB, and the elemental distributions of (c) SDB and (d) SDFB.

Table 6

The chemical elements of SDB and SDFB.

Materials	Chemical elements (%wt)					
	C	O	Ca	Cl	Na	Fe
SDB	45.9	35.6	16.4	1.5	0.6	–
SDFB	36.7	32.3	15.6	1.3	0.5	13.6

orbital shaker at 150 rpm for 6 h at room temperature. After that, they were filtrated and rinsed with deionized water, and they were air-dried. They were used for another adsorption cycle. Equation (2) is used to calculate the percentage of desorption efficiency.

$$\text{Desorption (\%)} = \left( \frac{q_d}{q_a} \right) \times 100 \quad (2)$$

where  $q_d$  is the amount of dye desorbed (mg/L) and  $q_a$  is the amount of dye adsorbed (mg/L).

### 2.8. Adsorption isotherms

Four isotherm models of Langmuir, Freundlich, Temkin, and Dubinin-Radushkevich in the linear and nonlinear are applied to identify the adsorption patterns of SDB and SDFB following Eqs. (3)–(10), and the good fit model is chosen with the highest  $R^2$  value. The details are displayed in Table 3.

For an isotherm lab, 3.5 g of SDB or 2.5 g of SDFB were added to 250 mL Erlenmeyer flasks with different DR28 dye concentrations from 40 to 80 mg/L, and used 200 mL of sample volume, 150 rpm of shaking speed, pH 3, 50 °C, and 12 h.

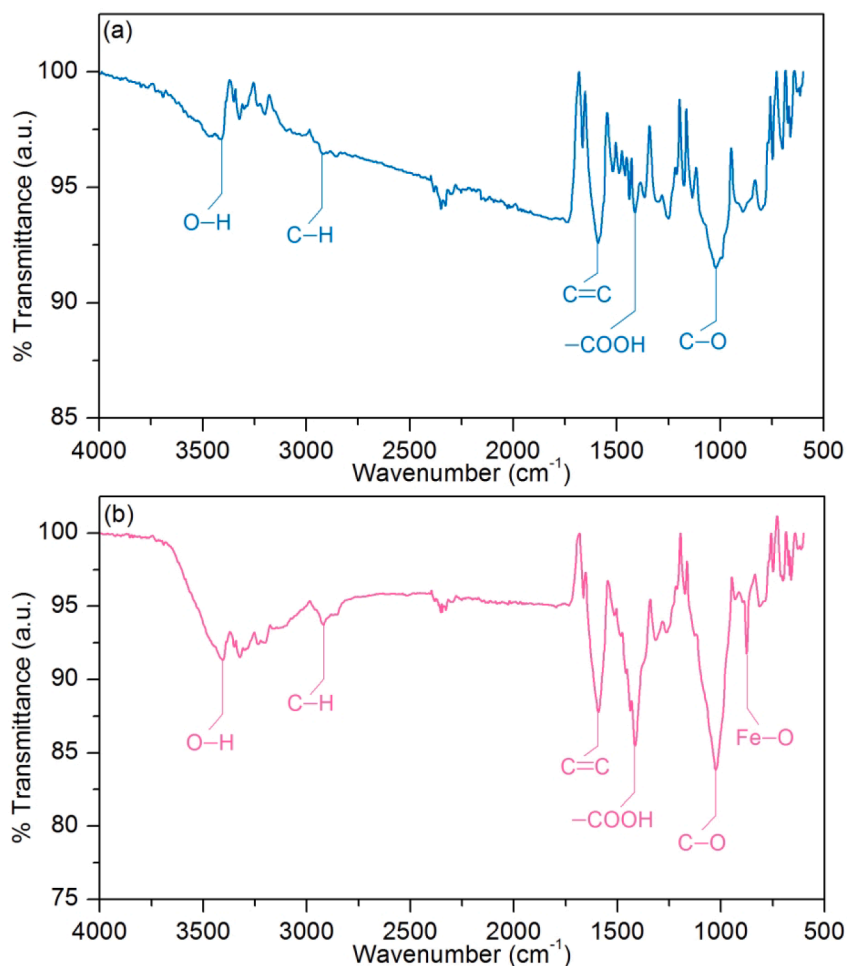


Fig. 4. FT-IR spectra of (a) SDB and (b) SDFB.

Table 7

The chemical functional groups of SDB and SDFB with wavenumber.

Wavenumber (cm <sup>-1</sup> )		Assignments	Functional groups	References
SDB	SDFB			
3413.76	3405.10	O—H	Hydroxyl, alcohol, and phenolic groups of lignin, cellulose, pectin, and fiber	(Rahman et al., 2021)
2935.55	2931.69	C—H	Methyl group (—CH <sub>2</sub> ) in cellulose and hemicellulose	(Essabir et al., 2016)
1664.51	1664.18	C=C	Aromatic rings of lignin	(Tejada-Tovar et al., 2021)
1417.63	1419.56	—COOH	Carboxyl group of sodium alginate	(Zhong et al., 2020)
1028.02	1029.95	C—O	Carboxylic acids of lignin and hemicellulose	(Rahman et al., 2021)
—	813.93	Fe—O	Metal-oxygen	(Praipipat et al., 2023b)

## 2.9. Adsorption kinetics

Four kinetic models of pseudo-first-order kinetic, pseudo-second-order kinetic, elovich, and intraparticle diffusion in the linear and nonlinear are used to investigate the adsorption mechanism of SDB and SDFB following Eqs. (11)–(18), and the model obtaining the highest  $R^2$  is selected similar to the criteria of a good fit model on the adsorption isotherm. The details are displayed in Table 4.

For a kinetic lab, 17.5 g of SDB or 12.5 g of SDFB were added to 1000 mL of breaker with a DR28 dye concentration of 60 mg/L, 1000 mL of sample volume, 150 rpm of shaking speed, pH 3, and 18 h with the ambient temperature for studying DR28 dye adsorptions.

## 2.10. Thermodynamic studies

Thermodynamic study is generally used for investigating how much the temperature affects the adsorption process by the adsorbent which the different temperatures from 303.15 to 343.15 K referred from the previous study (Praipipat et al., 2023b) were applied to explore the temperature effect on DR28 dye removals of SDB and SDFB using Eqs. (19)–(21) to determine their thermodynamic parameters (MacQueen, 1967).

$$\Delta G^\circ = -RT \ln K_c \quad (19)$$

where  $R$  is the universal gas constant (8.314 J/mol K),  $T$  is the absolute temperature (K), and  $K_c$  is the equilibrium constant (L/mg).

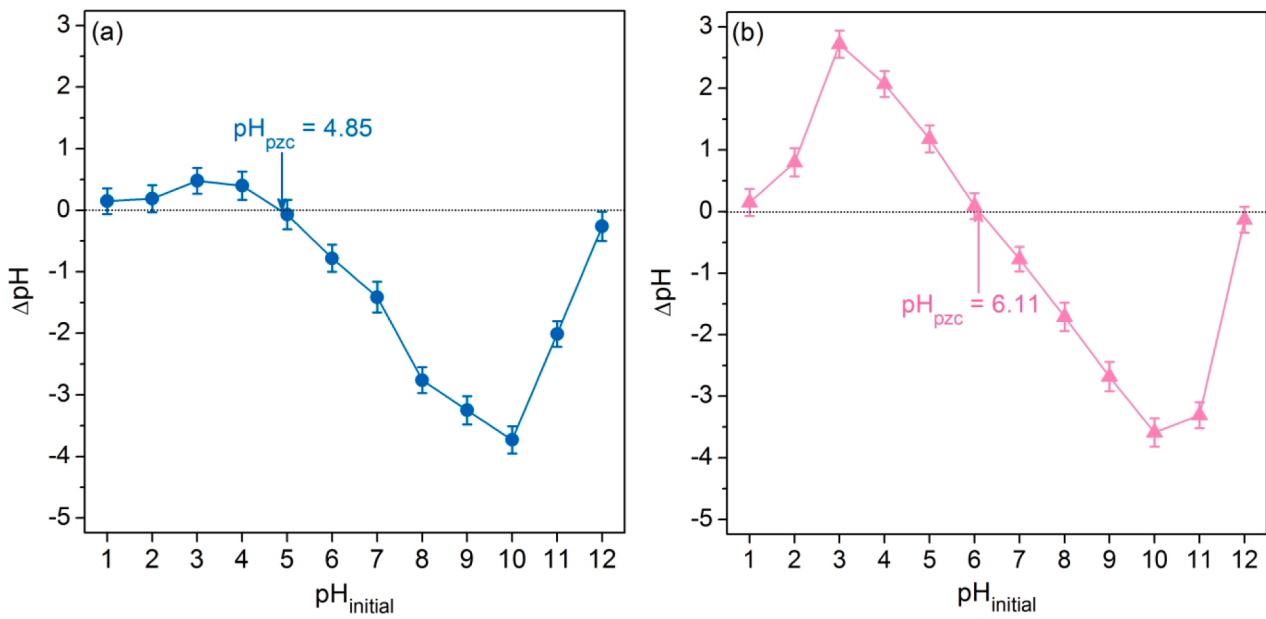


Fig. 5. The point of zero charges of (a) SDB and (b) SDFB.

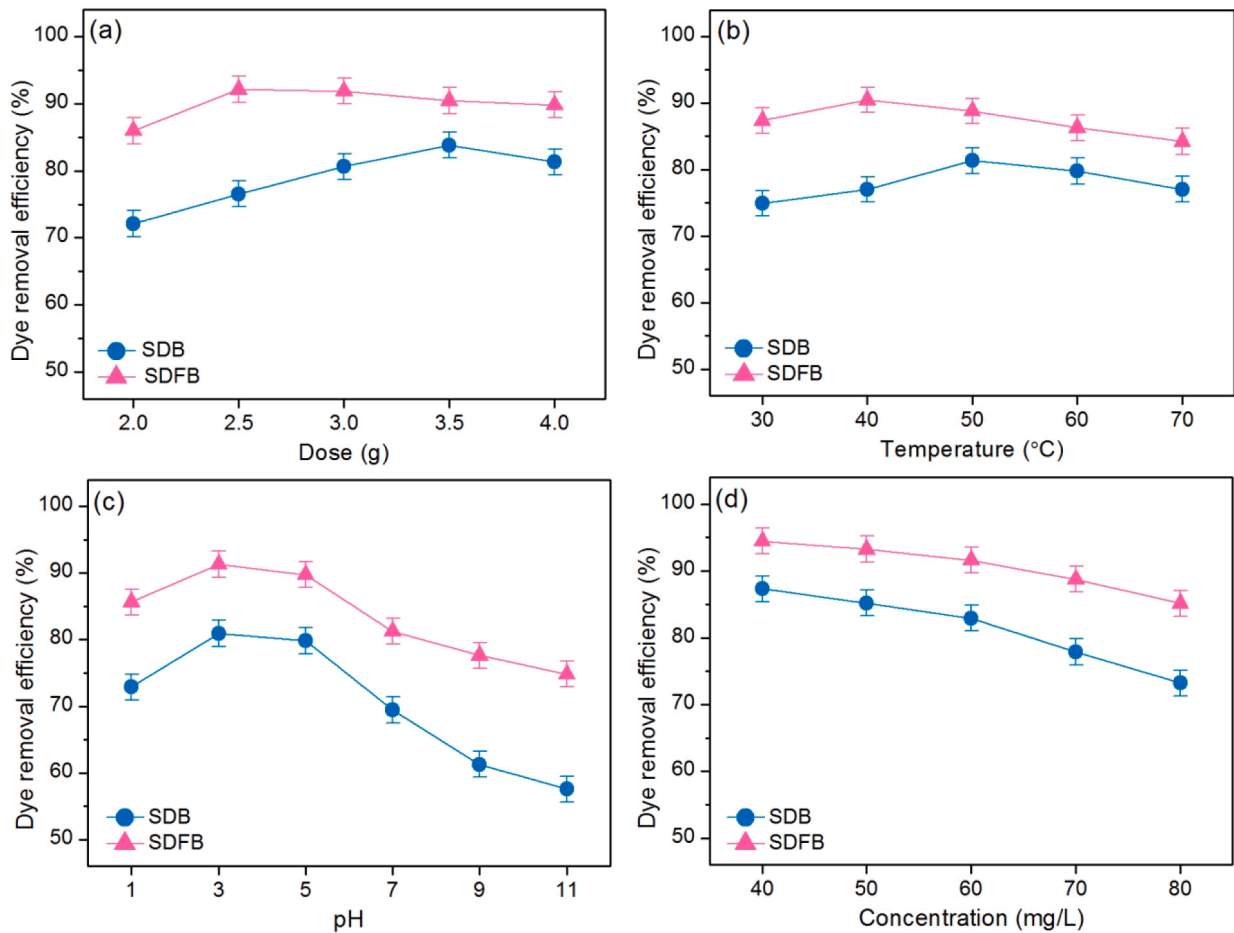


Fig. 6. Batch tests for DR28 dye removals on the effects of (a) dose, (b) temperature, (c) pH, and (d) concentration of SDB and SDFB.

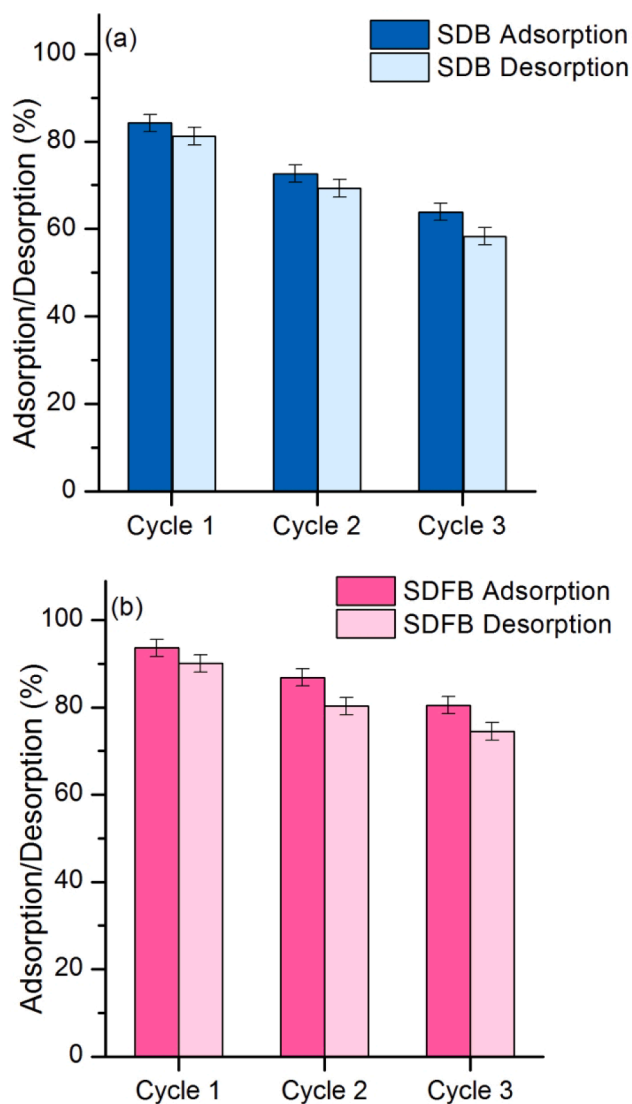


Fig. 7. The desorption tests of (a) SDB and (b) SDFB.

$$\ln K_c = -\frac{\Delta H^\circ}{RT} + \frac{\Delta S^\circ}{R} \quad (20)$$

$$\Delta G^\circ = \Delta H^\circ - T\Delta S^\circ \quad (21)$$

where  $\Delta H$  and  $\Delta S$  values were calculated from the slope and intercept of the linear graph between  $\ln K_c$  ( $K_c = q_e/C_e$ ) and  $1/T$ .

For the thermodynamic lab, 3.5 g of SDB or 2.5 g of SDFB were used with different temperatures from 303.15 to 343.15 K with a DR28 dye concentration of 60 mg/L, 200 mL of sample volume, 150 rpm of shaking speed, 12 h, and pH 3.

### 3. Result and discussion

#### 3.1. The physical characteristics

The physical characteristics of SDB and SDFB are shown in Fig. 2a and b. They were spherical with a brown color corresponding to the color of sawdust, whereas SDB was a brighter brown color bead than SDFB. Thus, the modification by iron(III) oxide-hydroxide affected the material color to be a darker brown color in SDFB.

#### 3.2. Material characterizations

##### 3.2.1. Brunauer-Emmett-Teller (BET)

BET analysis is used for investigating the physicochemical properties of SDB and SDFB by Barrett-Joyner-Halenda (BJH) method shown in Table 5. The specific surface area, pore volume, and pore size of SDB were 1.138 m<sup>2</sup>/g, 0.301 cm<sup>3</sup>/g, and 4.634 nm, and the specific surface area, pore volume, and pore size of SDFB were 12.540 m<sup>2</sup>/g, 2.714 cm<sup>3</sup>/g, and 4.306 nm which they were closely values with another previous study from sawdust materials (Praipipat et al., 2023b). From these results, SDFB had a higher specific surface area with a smaller pore size than SDB which was a good characteristic of an adsorbent for a high dye removal. Thus, the iron(III) oxide-hydroxide modification highly supported the DR28 dye removal similar found in other previous studies that used iron(III) oxide-hydroxide to increase the material capacity (Praipipat et al., 2023g, 2023a, 2023e, 2023c).

##### 3.2.2. Field Emission Scanning Electron Microscopy and Focus Ion Beam (FESEM-FIB) with Energy Dispersive X-Ray Spectrometer (EDX)

The surface structures of SDB and SDFB by FESEM-FIB at 1500X magnification with 100 μm are examined in Fig. 3a and b. The surface area of SDB and SDFB were uneven shapes and heterogeneous fibrillar structures corresponding to a wood structure similar to those observed in a previous study (Praipipat et al., 2023b).

The chemical elements of SDB and SDFB are illustrated in Table 6 consisting of carbon (C), oxygen (O), calcium (Ca), chloride (Cl), and sodium (Na), while iron (Fe) was found in SDFB from modifying by iron (III) oxide-hydroxide corresponded to a previous study (Praipipat et al., 2023b). Moreover, their elemental mapping is demonstrated in Fig. 3c and d to verify the five main chemical elements of C, O, Ca, Cl, and Na detected in both materials and found they spread over their surfaces. Furthermore, SDFB also found the Fe distribution on its surface confirmed the addition of iron(III) oxide-hydroxide into SDFB.

##### 3.2.3. Fourier Transform Infrared Spectroscopy (FT-IR)

The chemical functional groups of SDB and SDFB are determined by FT-IR, and their main chemical functional groups shown in FT-IR spectra are illustrated in Fig. 4a and b. In addition, the specific wavenumber of each chemical functional group in each material is illustrated in Table 7.

##### 3.2.4. The point of zero charge

The points of zero charge ( $pH_{pzc}$ ) of SDB and SDFB were 4.85 and 6.11, respectively demonstrated in Fig. 5a and b which iron(III) oxide-hydroxide could modify the sawdust material by increasing  $pH_{pzc}$  similarly observed in many studies (Ngamsurach et al., 2022; Praipipat et al., 2022b, 2023f, 2023a). Therefore, the pH of the sample solution ( $pH_{solution}$ ) <  $pH_{pzc}$  should be the appropriate pH for DR28 dye adsorptions of SDB and SDFB corresponding to the occurrence of anionic dye adsorption and the previous study reported (Praipipat et al., 2023d).

#### 3.3. Batch tests

The batch tests of SDB and SDFB for DR28 dye adsorptions are shown in Fig. 6a–d which demonstrated the optimum dose, temperature, pH, and concentration of SDB and SDFB were 3.5 g, 50 °C, pH 3, 60 mg/L for 82.93 % and 2.5 g, 40 °C, pH 3, 60 mg/L for 91.64 %, respectively. SDFB illustrated a higher DR28 dye removal than SDB by spending less dosage and temperature than SDB obtaining a higher DR28 dye removal than SDB. Therefore, the modification by iron(III) oxide-hydroxide in sawdust material resulted in increased DR28 dye removal efficiency.

#### 3.4. The adsorption–desorption tests

The adsorption–desorption tests of SDB and SDFB for removing DR28 dye in three cycles are reported in Fig. 7a and b. In three cycles, SDB had the percentages of adsorption–desorption in ranges of 63.87–84.23 %

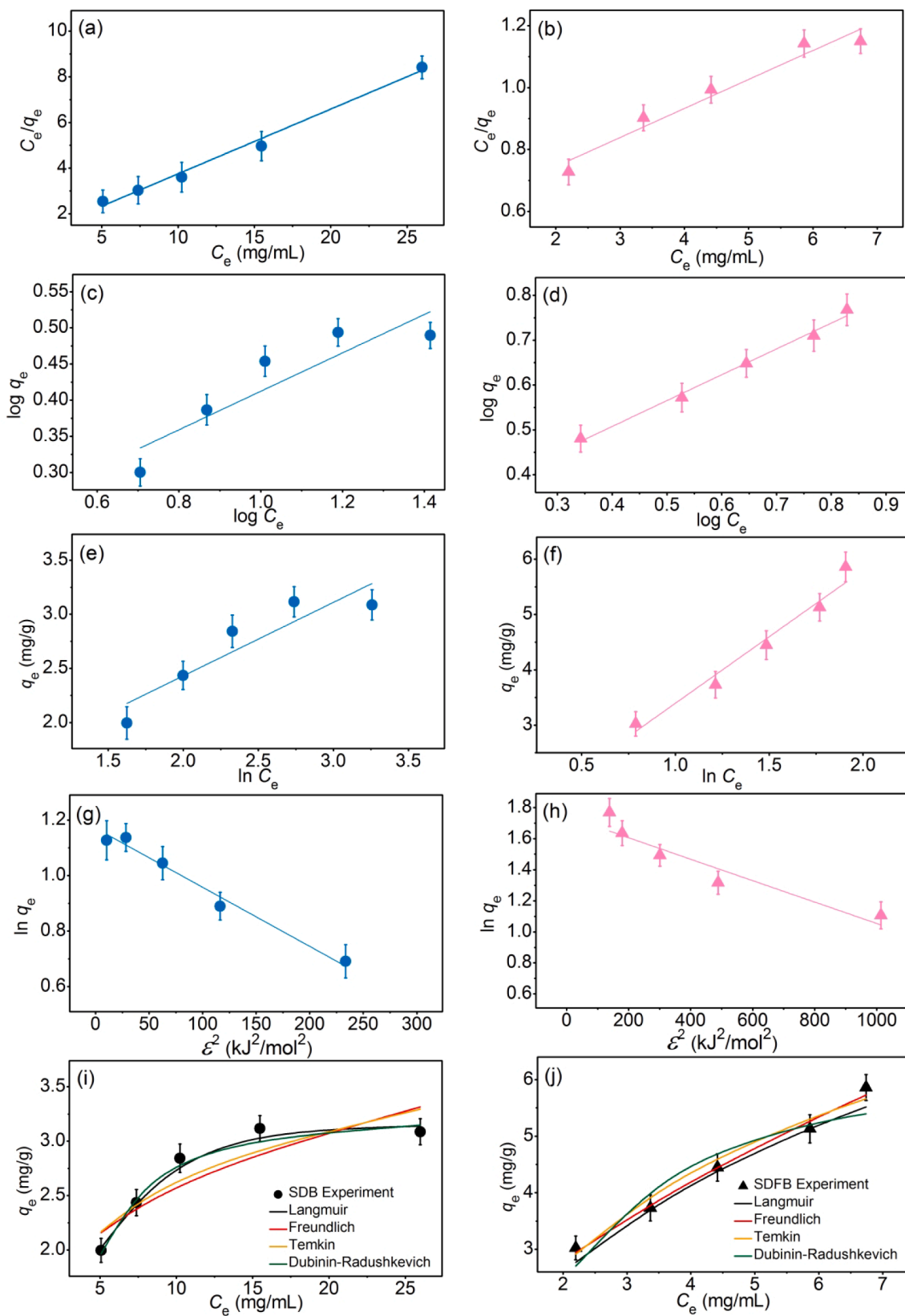


**Fig. 8.** Graphs of (a and b) linear Langmuir, (c and d) linear Freundlich, (e and f) linear Temkin, (g and h) linear Dubinin- Radushkevich, and (i and j) nonlinear adsorption isotherms of SDB and SDFB for DR28 dye adsorptions.

**Table 8**  
Linear and nonlinear isotherm parameters for DR28 dye adsorptions on SDB and SDFB.

Regression methods	Isotherm models	Parameters	SDB	SDFB
Linear	Langmuir	$q_m$ (mg/g)	3.534	10.593
		$K_L$ (L/mg)	0.321	0.170
		$R^2$	0.991	0.957
	Freundlich	$1/n$	0.269	0.580
		$K_F$ (mg/g)(L/mg) <sup>1/n</sup>	1.399	1.884
		$R^2$	0.823	0.993
	Temkin	$b_T$ (J/mol)	3896.547	1094.188
		$A_T$ (L/g)	4.573	1.455
		$R^2$	0.845	0.969
	Dubinin-Radushkevich	$q_m$ (mg/g)	3.208	5.800
		$K_{DR}$ (mol <sup>2</sup> /J <sup>2</sup> )	0.002	0.001
		$E$ (kJ/mol)	15.430	26.726
		$R^2$	0.982	0.898
	Nonlinear	Langmuir	$q_m$ (mg/g)	3.581
$K_L$ (L/mg)			0.388	0.160
$R^2$			0.993	0.963
$R_{adj}^2$			0.991	0.950
RMSE			0.044	0.249
Freundlich		$1/n$	0.262	0.595
		$K_F$ (mg/g)(L/mg) <sup>1/n</sup>	1.410	1.840
		$R^2$	0.819	0.990
		$R_{adj}^2$	0.759	0.987
		RMSE	0.253	0.126
Temkin		$b_T$ (J/mol)	3755.320	1026.477
		$A_T$ (L/g)	4.572	1.488
		$R^2$	0.848	0.966
		$R_{adj}^2$	0.798	0.955
		RMSE	0.217	0.238
Dubinin-Radushkevich		$q_m$ (mg/g)	3.216	6.020
		$K_{DR}$ (mol <sup>2</sup> /J <sup>2</sup> )	0.002	0.001
		$E$ (kJ/mol)	15.399	25.138
		$R^2$	0.979	0.891
		$R_{adj}^2$	0.972	0.854
		RMSE	0.080	0.427

and 58.30–81.22 % decreasing by 22.36 % and 22.92 %. While SDFB had the percentages of adsorption–desorption in ranges of 80.49–93.61 % and 74.48–90.11 % decreasing by 13.12 % and 15.63 %. As a result, SDFB had a higher DR28 dye adsorption than SDF corresponding to batch test results. Therefore, SDB and SDFB could reuse more than three cycles with high DR28 dye adsorptions of more than 63 %. For the evaluation of cost-effectiveness, not only SDB and SDFB could reuse more than three cycles with high DR28 dye adsorptions but also the use of sawdust from a sawmill could reuse waste and increase the value of waste by reusing it as a dye absorbent. Moreover, the material synthesis costs of SDB and SDFB were suitable costs of approximately 25 USD per kg. In addition, since SDB and SDFB are beaded materials, they are easy to separate from treated wastewater and reduce the operating cost of wastewater treatment. Therefore, they are potential materials for the feasibility of industrial applications for removing DR28 dye in wastewater, especially SDFB.

### 3.5. Adsorption isotherms

The adsorption isotherms of SDB and SDFB for eliminating DR28 dye are shown in Fig. 8a–j and Table 8 which good fit models of SDB and SDFB were Langmuir and Freundlich, respectively. Therefore, SDB was the physical adsorption, while SDFB was the physiochemical adsorption. In addition, the linear and nonlinear plotting graphs are recommended to protect against data mistranslation similarly supported by previous studies (Ngamsurach et al., 2022; Praipipat et al., 2023b).

In comparison, the maximum adsorption capacities of several waste adsorbents with or without modifications for DR28 dye removals are demonstrated and compared with this study in Table 9. SDFB examined the highest DR28 dye removal than other studies, whereas SDB showed a higher DR28 dye removal than waste adsorbents of rice husk, banana peel, cabbage, and sugarcane bagasse fly ash. Therefore, SDFB was a potential material for DR28 dye adsorption in industrial applications.

**Table 9**  
The maximum adsorption capacity for DR28 dye adsorptions by various waste adsorbents.

Materials	Conditions	$q_m$ (mg/g)	References
Rice husk char	0.5 g, 20 min, 30 °C, pH 4, concentration 20–100 mg/L, 15 mL	1.28	(Malik et al., 2020)
Rice husk	0.5 g, 20 min, 30 °C, pH 4, concentration 20–100 mg/L, 15 mL	1.58	(Malik et al., 2020)
Rice husk char modified potassium hydroxide	0.5 g, 20 min, 30 °C, pH 6, concentration 20–100 mg/L, 15 mL	2.04	(Malik et al., 2020)
Banana peel	1.5 g, 1.5 h, 40 °C, pH 10, concentration 20–40 mg/L, 80 mL	1.72	(Mondal and Kar, 2018)
Cabbage	2.0 g, 3 h, 25 °C, pH 8, concentration 4.88–48.76 mg/L, 50 mL	2.31	(Wekoye et al., 2020)
Pine bark	10 g/L, 25 °C, pH 6, concentration 5–100 mg/L, 100 mL	3.92	(Litefti et al., 2019)
Calcined kaolin	1.2 g, 2 h, 20 °C, concentration 20–50 mg/L, 200 mL	5.39	(Findik, 2023)
Sugarcane bagasse fly ash beads	2.5 g, 15 h, 30 °C, pH 3, concentration 30–90 mg/L, 100 mL	3.36	(Praipipat et al., 2023d)
Sugarcane bagasse fly ash beads doped with zinc oxide	2.5 g, 12 h, 30 °C, pH 3, concentration 30–90 mg/L, 100 mL	3.90	(Praipipat et al., 2023d)
Sugarcane bagasse fly ash beads doped with titanium dioxide	2.0 g, 15 h, 30 °C, pH 3, concentration 30–90 mg/L, 100 mL	4.01	(Praipipat et al., 2023d)
Sugarcane bagasse fly ash beads doped with aluminum oxide	1.5 g, 15 h, 30 °C, pH 3, concentration 30–90 mg/L, 100 mL	5.46	(Praipipat et al., 2023d)
Sugarcane bagasse fly ash beads doped with magnesium oxide	1.5 g, 12 h, 30 °C, pH 3, concentration 30–90 mg/L, 100 mL	5.56	(Praipipat et al., 2023d)
SDB	3.5 g, 12 h, 50 °C, pH 3, concentration 40–80 mg/L, 200 mL	3.53	This study
SDFB	2.5 g, 12 h, 50 °C, pH 3, concentration 40–80 mg/L, 200 mL	10.59	This study

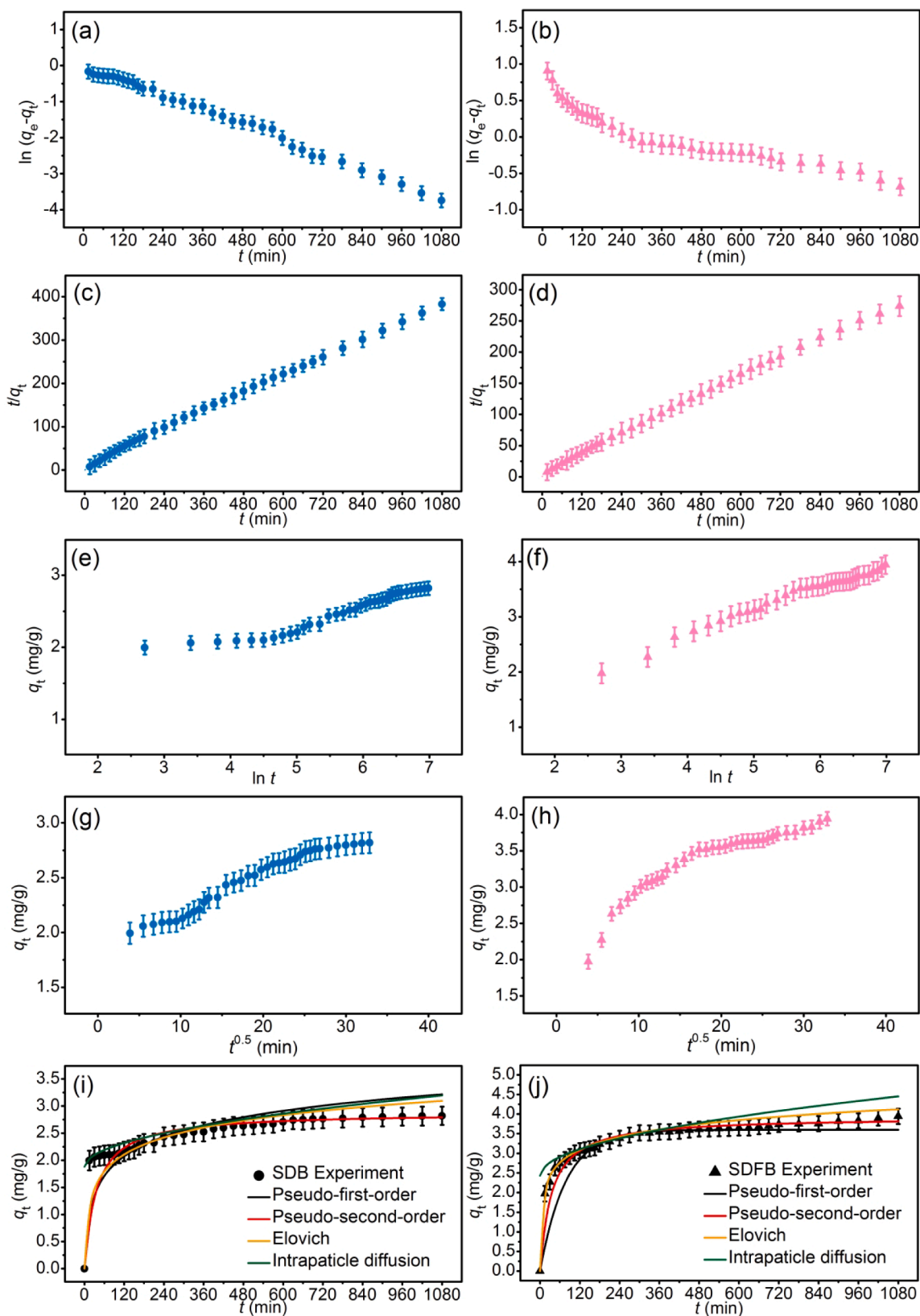


Fig. 9. Graphs of (a and b) linear pseudo-first-order, (c and d) linear pseudo-second-order, (e and f) linear elovich model (g and h) linear intraparticle diffusion, and (i and j) nonlinear kinetic models of SDB and SDFB for DR28 dye adsorptions.

**Table 10**  
Linear and nonlinear kinetic parameters for DR28 dye adsorptions on SDB and SDFB.

Regression methods	Kinetic models	Parameters	SDB	SDFB
Linear	Pseudo-first-order	$q_e$ (mg/g)	1.117	1.617
		$k_1$ ( $\text{min}^{-1}$ )	0.003	0.001
		$R^2$	0.968	0.869
	Pseudo-second-order	$q_e$ (mg/g)	2.881	3.931
		$k_2$ (g/mg.min)	0.010	0.008
		$R^2$	0.998	0.998
	Elovich	$\alpha$ (mg/g.min)	5.096	14.999
		$\beta$ (g/mg)	3.015	2.362
		$R^2$	0.904	0.981
	Intraparticle diffusion	$k_i$ (mg/g.min <sup>0.5</sup> )	0.033	0.052
		$C_i$	1.862	2.396
		$R^2$	0.963	0.858
Nonlinear	Pseudo-first-order	$q_e$ (mg/g)	1.550	1.812
		$k_1$ ( $\text{min}^{-1}$ )	0.004	0.002
		$R^2$	0.965	0.871
		$R_{\text{adj}}^2$	0.964	0.867
		RMSE	0.391	0.408
	Pseudo-second-order	$q_e$ (mg/g)	2.895	3.927
		$k_2$ (g/mg.min)	0.013	0.009
		$R^2$	0.996	0.939
		$R_{\text{adj}}^2$	0.995	0.938
		RMSE	0.231	0.179
	Elovich	$\alpha$ (mg/g.min)	5.148	15.270
		$\beta$ (g/mg)	3.451	2.470
		$R^2$	0.906	0.985
		$R_{\text{adj}}^2$	0.903	0.984
		RMSE	0.228	0.143
	Intraparticle diffusion	$k_i$ (mg/g.min <sup>0.5</sup> )	0.036	0.061
		$C_i$	1.879	2.432
		$R^2$	0.966	0.863
		$R_{\text{adj}}^2$	0.965	0.859
		RMSE	0.361	0.503

### 3.6. Adsorption kinetics

The adsorption kinetics of SDB and SDFB for adsorbing DR28 dye are examined in Fig. 9a–j and Table 10. SDB and SDFB corresponded to the pseudo-second-order model which meant their adsorption mechanism was the chemisorption process that corresponded to many studies (Ngamsurach et al., 2022; Praipipat et al., 2022b, 2023b). In addition, the linear and nonlinear kinetic models corresponded to each other similarly to the adsorption isotherm results, so they were correct data translations in this study.

### 3.7. Thermodynamic studies

The thermodynamic studies of SDB and SDFB for DR28 dye adsorptions are illustrated in Table 11. In addition, their thermodynamic plots for DR28 dye adsorptions used to determine the values of  $\Delta H^\circ$  and  $\Delta S^\circ$  from the slope and intercept of their linear equations plotted by  $\ln K_c$  versus  $1/T$  are demonstrated in Fig. 10a and b. If the slope is a positive value,  $\Delta H^\circ$  is a negative value meaning the exothermic process. In addition, if the intercept is a negative value,  $\Delta S^\circ$  is a negative value meaning the decreasing of randomness during the adsorption process. Since their  $\Delta G^\circ$  values were negative which were favorable adsorption processes of a spontaneous nature. For  $\Delta H^\circ$  and  $\Delta S^\circ$ , both SDB and SDFB were also negative which were exothermic in nature (Praipipat et al.,

2022b) and decreased the randomness during the adsorption process (Wong et al., 2019). Thus, DR28 dye adsorptions of both materials were not favorable when the temperature increased.

## 4. The possible mechanisms of SDB and SDFB for DR28 dye adsorptions

The possible mechanisms of SDB and SDFB for adsorbing DR28 dye could be explained by modifying ideas from the previous studies of Ngamsurach et al. (Ngamsurach et al., 2022) and Praipipat et al. (Praipipat et al., 2023b) which the electrostatic attraction, hydrogen bonding interaction, and  $n-\pi$  bonding interaction were main mechanisms of DR28 dye adsorptions. In addition, their main chemical functional groups of hydroxyl ( $-\text{OH}$ ) and iron(III) oxide-hydroxide ( $-\text{Fe}(\text{OH})_3$ ) occurring from sharing the electron with  $-\text{OH}$  had an important role in their adsorption mechanisms clearly described in Fig. 11a and b. For the electrostatic attraction, the positively charged of  $-\text{OH}$  on SDB and SDFB surfaces interacted with the negatively charged of sulfonate groups ( $-\text{SO}_3^-$ ) of DR28 dye at an acidic solution which its  $\text{pH} < \text{pH}_{\text{pzc}}$  of SDB and SDFB illustrated in Fig. 5a and b. For the hydrogen bonding interaction, the hydrogen ions in  $-\text{OH}$  caught up with the nitrogen ions in the DR28 dye. Finally, the oxygen atom in  $-\text{OH}$  interacted with the aromatic ring in the DR28 dye demonstrating the  $n-\pi$  bonding interaction.

**Table 11**  
Thermodynamic parameters of SDB and SDFB for DR28 dye removals.

Materials	$\Delta G^\circ$ (kJ/mol)					$\Delta H^\circ$ (kJ/mol)	$\Delta S^\circ$ (J/mol K)
	303.15 K	313.15 K	323.15 K	333.15 K	343.15 K		
SDB	-1.23	-0.97	-0.75	-0.45	-0.21	-8.96	-25.49
SDFB	-3.98	-3.47	-3.10	-2.55	-2.17	-17.79	-45.61

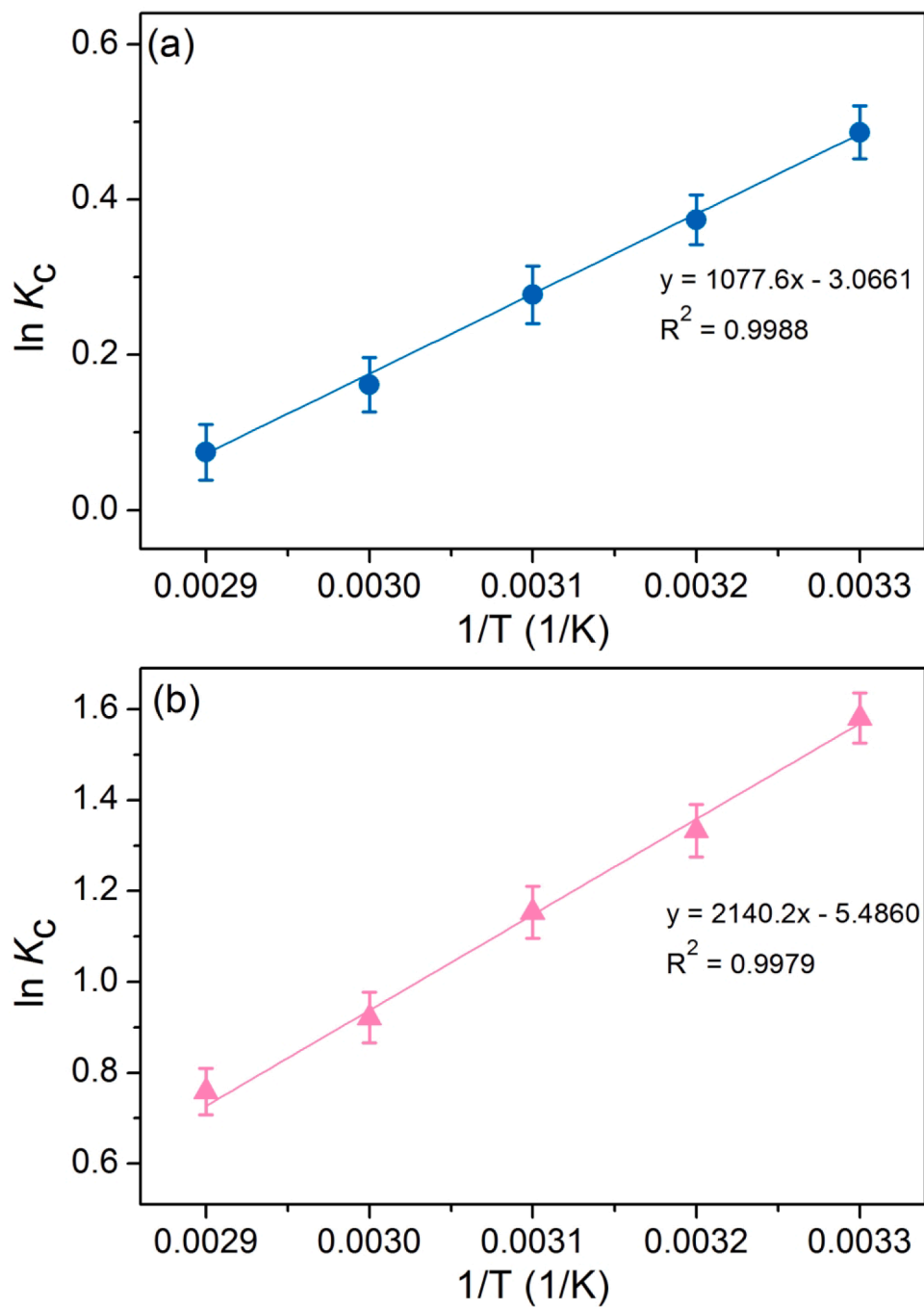


Fig. 10. Thermodynamic plots of (a) SDB and (b) SDFB for DR28 dye adsorptions.

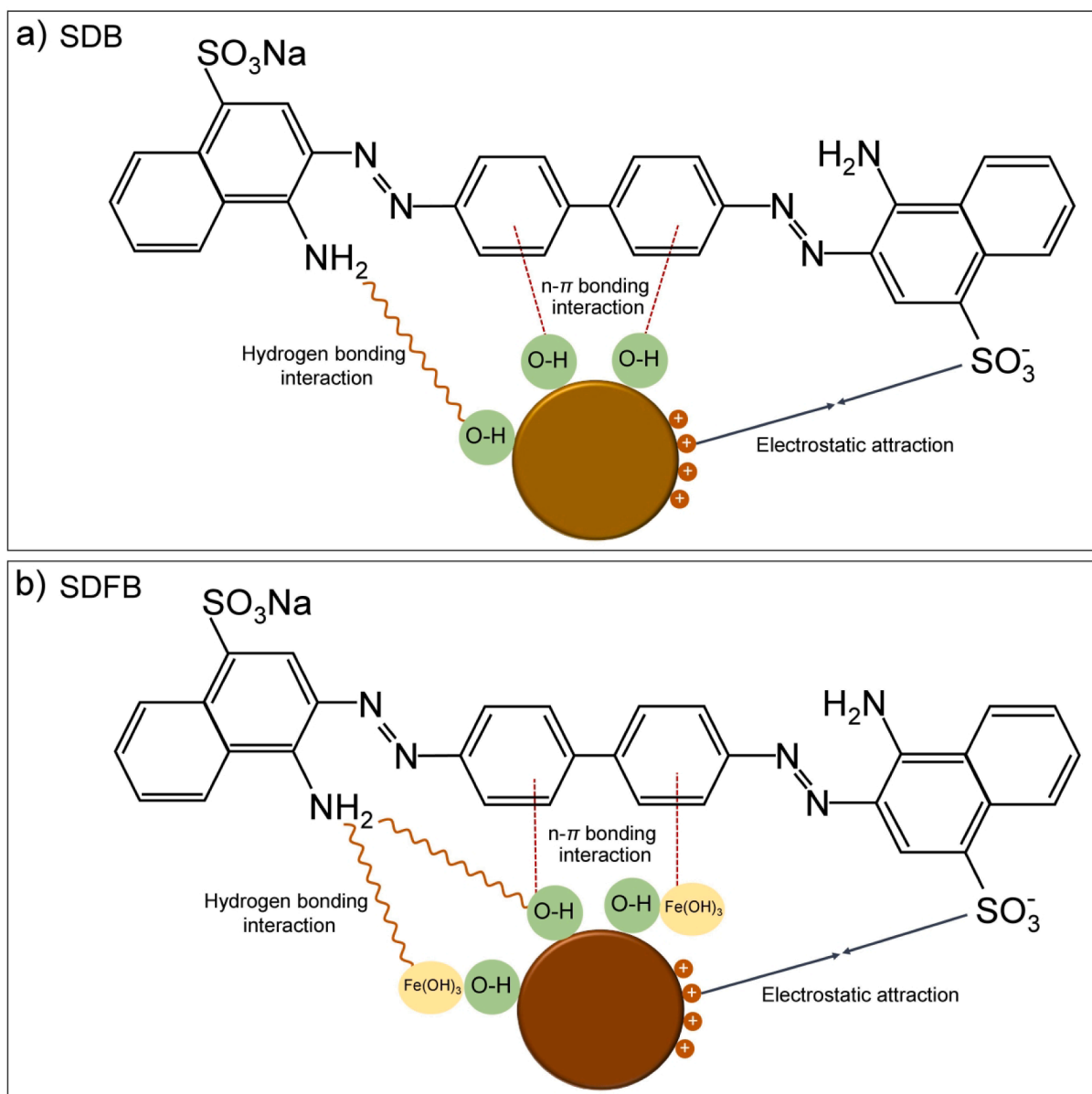


Fig. 11. Possible mechanisms of DR28 dye adsorptions on (a) SDB and (b) SDFB.

## 5. Conclusion

*Pterocarpus macrocarpus* sawdust was used for synthesizing sawdust beads (SDB) and sawdust mixed with iron(III) oxide-hydroxide beads (SDFB) for DR28 dye adsorptions. Iron(III) oxide-hydroxide increased sawdust material efficiency by increasing the specific surface area to be more available DR28 dye adsorptions, and the batch test results also confirmed a higher DR28 dye removal of SDFB of 91.64 % than SDB of 82.93 % which SDFB also spent material dose and temperature less than SDB. Moreover, they also reused more than three cycles with high DR28 dye adsorptions of more than 63 %. Their DR28 dye adsorptions were an exothermic process that did not favor adsorption with increasing temperature. Three possible mechanisms of electrostatic attraction, hydrogen bonding interaction, and  $n-\pi$  bonding interaction could be good explanations for their DR28 dye adsorptions. Therefore, they are potential sawdust materials for removing DR28 dye contaminated in wastewater, especially SDFB.

For future works, the column experiments need to be studied before being applied in industry, and the competing ions might be necessary to explore their DR28 dye removal efficiencies of SDB and SDFB in case of real wastewater to confirm specific DR28 dye removals by them.

## CRediT authorship contribution statement

**Pornsawai Praipipat:** Supervision, Conceptualization, Investigation, Methodology, Validation, Visualization, Writing – original draft, Writing – review & editing. **Pimpoy Ngamsurach:** Investigation, Visualization, Writing – original draft. **Piyaporn Khamkhae:** Investigation.

## Declaration of competing interest

The authors declare that they have no known competing financial interests or personal relationships that could have appeared to influence the work reported in this paper.

## References

- Abdel-Aziz, M.H., El-Ashtouky, E.Z., Bassyouni, M., Al-Hossainy, A.F., Fawzy, E.M., Abdel-Hamid, S.M.S., Zoromba, M.S., 2021. DFT and experimental study on adsorption of dyes on activated carbon prepared from apple leaves. *Carbon Lett.* 31, 863–878. <https://doi.org/10.1007/s42823-020-00187-1>.

- Ahamad, Z., Nasar, A., 2023. Utilization of *Azadirachta indica* sawdust as a potential adsorbent for the removal of crystal violet dye. *Sustain. Chem.* 4, 110–126. <https://doi.org/10.3390/suschem4010009>.
- Ahamad, R., Ansari, K., 2021. Comparative study for adsorption of congo red and methylene blue dye on chitosan modified hybrid nanocomposite. *Process Biochem.* 108, 90–102. <https://doi.org/10.1016/j.procbio.2021.05.013>.
- Benkhaya, S., Mrabet, S., El Harfi, A., 2020. Classifications, properties, recent synthesis and applications of azo dyes. *Heliyon* 6, e03271.
- Bukhari, A., Ijaz, I., Zain, H., Gilani, E., Nazir, A., Bukhari, A., Raza, S., Hussain, S., Alarfajji, S.S., Naseer, Y., Aftab, R., 2022. Removal of Eosin dye from simulated media onto lemon peel-based low cost biosorbent. *Arab. J. Chem.* 15, 103873 <https://doi.org/10.1016/j.arabjc.2022.103873>.
- Değermenci, G.D., Değermenci, N., Ayyavoglu, V., Durmaz, E., Çakır, D., Akan, E., 2019. Adsorption of reactive dyes on lignocellulosic waste; characterization, equilibrium, kinetic and thermodynamic studies. *J. Clean. Prod.* 225, 1220–1229. <https://doi.org/10.1016/j.jclepro.2019.03.260>.
- Dubinina, M.M., Radushkevich, L.V., 1947. The equation of the characteristic curve of activated charcoal. *Proc. USSR Acad. Sci.* 55, 327–329.
- Dutta, S., Gupta, B., Srivastava, S.K., Gupta, A.K., 2021. Recent advances on the removal of dyes from wastewater using various adsorbents: a critical review. *Mater. Adv.* 2, 4497–4531. <https://doi.org/10.1039/d1ma00354b>.
- Ebrahimian Pirbazari, A., Saberikhah, E., Habibzadeh Kozani, S.S., 2014. Fe<sub>3</sub>O<sub>4</sub>-wheat straw: preparation, characterization and its application for methylene blue adsorption. *Water Resour. Ind.* 7–8, 23–37. <https://doi.org/10.1016/j.wri.2014.09.001>.
- Elovich, S.Y., Larinov, O.G., 1962. Theory of adsorption from solutions of non electrolytes on solid (I) equation adsorption from solutions and the analysis of its simplest form, (II) verification of the equation of adsorption isotherm from solutions. *Izv. Akad. Nauk. SSSR Ord. Khim. Nauk* 2, 209–216.
- Esmaili, H., Foroutan, R., 2019. Adsorptive behavior of methylene blue onto sawdust of sour lemon, date palm, and eucalyptus as agricultural wastes. *J. Dispers. Sci. Technol.* 40, 990–999. <https://doi.org/10.1080/01932691.2018.1489828>.
- Essabir, H., Boujmal, R., Bensalah, M.O., Rodrigue, D., Bouhfid, R., Qaiss, A.E.K., 2016. Mechanical and thermal properties of hybrid composites: oil-palm fiber/clay reinforced high density polyethylene. *Mech. Mater.* 98, 36–43. <https://doi.org/10.1016/j.mechmat.2016.04.008>.
- Farahani, M., Kashisaz, M., Abdullah, S.R.S., 2015. Adsorption of safranin O from aqueous phase using sugarcane bagasse. *Int. J. Ecol. Sci. Environ. Eng.* 2, 17–29.
- Findik, S., 2023. Adsorption of diazo dye direct red-28 and tetra-azo dye direct black-22 using calcined kaolin in aqueous solutions. *Bull. Chem. Soc. Ethiop.* 37, 593–610.
- Foroutan, R., Mohammadi, R., Ahmadi, A., Bikhbar, G., Babaei, F., Ramavandi, B., 2022. Impact of ZnO and Fe<sub>3</sub>O<sub>4</sub> magnetic nanoscale on the methyl violet 2B removal efficiency of the activated carbon oak wood. *Chemosphere* 286, 131632. <https://doi.org/10.1016/j.chemosphere.2021.131632>.
- Freundlich, H., 1906. Over the adsorption in solution. *J. Phys. Chem.* 57, 385–470. <https://doi.org/10.1515/zpch-1907-5723>.
- Fu, F., Gao, Z., Gao, L., Li, D., 2011. Effective adsorption of anionic dye, alizarin red S, from aqueous solutions on activated clay modified by iron oxide. *Ind. Eng. Chem. Res.* 50, 9712–9717. <https://doi.org/10.1021/ie200524b>.
- Guechi, E.-K., Benabdesselam, S., Hamdaoui, O., 2021. Biosorption of methyl violet 2B by chemically treated Okoume sawdust: kinetic, isotherm and thermodynamic studies. *Alger. J. Eng. Res.* 4, 34–41.
- Gul, S., Kanwal, M., Qazi, R.A., Gul, H., Khattak, R., Khan, M.S., Khitab, F., Krauklis, A. E., 2022. Efficient removal of methyl red dye by using bark of hophbush. *Water* 14, 2831. <https://doi.org/10.3390/w14182831>.
- Harja, M., Buema, G., Bucur, D., 2022. Recent advances in removal of Congo Red dye by adsorption using an industrial waste. *Sci. Rep.* 12, 6087. <https://doi.org/10.1038/s41598-022-10093-3>.
- Ho, Y.S., McKay, G., 1999. Pseudo-second order model for sorption processes. *Process Biochem.* 34, 451–465. [https://doi.org/10.1016/S0032-9592\(98\)00112-5](https://doi.org/10.1016/S0032-9592(98)00112-5).
- Iqbal, M.M., Imran, M., Hussain, T., Naeem, M.A., Al-Kahtani, A.A., Shah, G.M., Ahmad, S., Farooq, A., Rizwan, M., Majeed, A., Khan, A.R., Ali, S., 2021. Effective sequestration of Congo red dye with ZnO/cotton stalks biochar nanocomposite: MODELING, reusability and stability. *J. Saudi Chem. Soc.* 25, 101176 <https://doi.org/10.1016/j.jscs.2020.101176>.
- Islam, T., Repon, M.R., Islam, T., Sarwar, Z., Rahman, M.M., 2023. Impact of textile dyes on health and ecosystem: a review of structure, causes, and potential solutions. *Environ. Sci. Pollut. Res.* <https://doi.org/10.1007/s11356-022-24398-3>.
- Khader, E.H., Mohammed, T.J., Albayati, T.M., 2021. Comparative performance between rice husk and granular activated carbon for the removal of azo tartrazine dye from aqueous solution. *Desalin. Water Treat.* 229, 372–383. <https://doi.org/10.5004/dwt.2021.27374>.
- Khalaf, I.H., Al-Sudani, F.T., AbdulRazak, A.A., Aldahri, T., Rohani, S., 2021. Optimization of Congo red dye adsorption from wastewater by a modified commercial zeolite catalyst using response surface modeling approach. *Water Sci. Technol.* 83, 1369–1383. <https://doi.org/10.2166/wst.2021.078>.
- Lagergren, S., 1898. About the theory of so-called adsorption of soluble substances. *K. Sven. Vetenskapsakademiens Handl.* 24, 1–39.
- Langmuir, I., 1918. The adsorption of gases on plane surfaces of glass, mica and platinum. *J. Am. Chem. Soc.* 40, 1361–1403.
- Litefti, K., Freire, M.S., Stitou, M., González-Álvarez, J., 2019. Adsorption of an anionic dye (Congo red) from aqueous solutions by pine bark. *Sci. Rep.* 9, 16530. <https://doi.org/10.1038/s41598-019-53046-z>.
- Loulihi, I., Boukhlifi, F., Ouchabi, M., Amar, A., Jabri, M., Kali, A., Chraïbi, S., Hadey, C., Aziz, F., 2020. Adsorption of crystal violet onto an agricultural waste residue: kinetics, isotherm, thermodynamics, and mechanism of adsorption. *Sci. World J.*, 5873521 <https://doi.org/10.1155/2020/5873521>.
- MacQueen, J.T., 1967. Some observations concerning the van't Hoff equation. *J. Chem. Educ.* 44, 755–756. <https://doi.org/10.1021/ed044p755>.
- Malik, A., Khan, A., Anwar, N., Muhammad, N., 2020. A comparative study of the adsorption of congo red dye on rice husk, rice husk char and chemically modified rice husk char from aqueous media. *Bull. Chem. Soc. Ethiop.* 34, 41–54.
- Mondal, N.K., Kar, S., 2018. Potentiality of banana peel for removal of Congo red dye from aqueous solution: isotherm, kinetics and thermodynamics studies. *Appl. Water Sci.* 8, 157. <https://doi.org/10.1007/s13201-018-0811-x>.
- Muinde, V.M., Onyari, J.M., Wamalwa, B., Wabomba, J.N., 2020. Adsorption of malachite green dye from aqueous solutions using mesoporous chitosan-zinc oxide composite material. *Environ. Chem. Ecotoxicol.* 2, 115–125. <https://doi.org/10.1016/j.enecoc.2020.07.005>.
- Muneer, I., Javed, T., Majeed, A.A., Masood, H.T., 2021. A brief study of adsorption of Congo red dye over sawdust of *Cedrus deodara*. *Desalin. Water Treat.* 235, 272–282. <https://doi.org/10.5004/dwt.2021.27596>.
- Ngamsurach, P., Nemkhuntod, S., Chanaphan, P., Praipipat, P., 2022. Modified beaded materials from recycled wastes of bagasse and bagasse fly ash with iron (III) oxide-hydroxide and zinc oxide for the removal of reactive blue 4 dye in aqueous solution. *ACS Omega* 7, 34839–34857. <https://doi.org/10.1021/acsomega.2c03250>.
- Oladoye, P.O., Bamigboye, M.O., Ogunbiyi, O.D., Akano, M.T., 2022. Toxicity and decontamination strategies of Congo red dye. *Groundw. Sustain. Dev.* 19, 100844 <https://doi.org/10.1016/j.gsd.2022.100844>.
- Oyewo, O.A., Adeniyi, A., Sithole, B.B., Onyango, M.S., 2020. Sawdust-based cellulose nanocrystals incorporated with ZnO nanoparticles as efficient adsorption media in the removal of methylene blue dye. *ACS Omega* 5, 18798–18807. <https://doi.org/10.1021/acsomega.0c01924>.
- Patabandige, D.S.B.T., Wadumethrige, S.H., Wanniarachchi, S., 2019. H<sub>3</sub>PO<sub>4</sub>-activated sawdust and rice husk as effective decolorizers for textile wastewater containing Reactive Black 5. *Int. J. Environ. Sci. Technol.* 16, 8375–8388. <https://doi.org/10.1007/s13762-019-02394-4>.
- Pooladi, H., Foroutan, R., Esmaili, H., 2021. Synthesis of wheat bran sawdust/Fe<sub>3</sub>O<sub>4</sub> composite for the removal of methylene blue and methyl violet. *Environ. Monit. Assess.* 193, 276. <https://doi.org/10.1007/s10661-021-09051-9>.
- Praipipat, P., Ngamsurach, P., Prasongdee, V., 2022a. Comparative reactive blue 4 dye removal by lemon peel bead doping with iron (III) oxide-hydroxide and zinc oxide. *ACS Omega* 7, 41744–41758. <https://doi.org/10.1021/acsomega.2c05956>.
- Praipipat, P., Ngamsurach, P., Saekrathok, C., Phomtai, S., 2022b. Chicken and duck eggshell beads modified with iron (III) oxide-hydroxide and zinc oxide for reactive blue 4 dye removal. *Arab. J. Chem.* 15, 104291 <https://doi.org/10.1016/j.arabjc.2022.104291>.
- Praipipat, P., Jangkorn, S., Ngamsurach, P., 2023a. Powdered and beaded zeolite A from recycled coal fly ash with modified iron (III) oxide-hydroxide for lead adsorptions. *Environ. Nanotechnol. Monit. Manag.* 20, 100812 <https://doi.org/10.1016/j.enmm.2023.100812>.
- Praipipat, P., Ngamsurach, P., Kosumphon, S., Mokkarat, J., 2023b. Powdered and beaded sawdust materials modified iron (III) oxide-hydroxide for adsorption of lead (II) ion and reactive blue 4 dye. *Sci. Rep.* 13, 531. <https://doi.org/10.1038/s41598-023-27789-9>.
- Praipipat, P., Ngamsurach, P., Pratumkaew, K., 2023c. The synthesis, characterizations, and lead adsorption studies of chicken eggshell powder and chicken eggshell powder-doped iron (III) oxide-hydroxide. *Arab. J. Chem.* 16, 104640 <https://doi.org/10.1016/j.arabjc.2023.104640>.
- Praipipat, P., Ngamsurach, P., Rattanavaru, M., Choothai, N., 2023d. Synthesis and characterization of metal oxide doped beaded sugarcane bagasse fly ash for direct red 28 dye removal. *J. Ind. Eng. Chem.* 25, 495–514. <https://doi.org/10.1016/j.jiec.2023.08.015>.
- Praipipat, P., Ngamsurach, P., Roopkhan, N., 2023e. Zeolite A powder and beads from sugarcane bagasse fly ash modified with iron(III) oxide-hydroxide for lead adsorption. *Sci. Rep.* 13, 1873. <https://doi.org/10.1038/s41598-023-29055-4>.
- Praipipat, P., Ngamsurach, P., Sanghuayprai, A., 2023f. Modification of sugarcane bagasse with iron(III) oxide-hydroxide to improve its adsorption property for removing lead(II) ions. *Sci. Rep.* 13, 1467. <https://doi.org/10.1038/s41598-023-28654-5>.
- Praipipat, P., Ngamsurach, P., Tannadee, R., 2023g. Influence of duck eggshell powder modifications by the calcination process or addition of iron (III) oxide-hydroxide on lead removal efficiency. *Sci. Rep.* 13, 12100. <https://doi.org/10.1038/s41598-023-39325-w>.
- Praipipat, P., Ngamsurach, P., Thanyahan, A., Sakda, A., 2023h. Reactive blue 4 adsorption efficiencies on bagasse and bagasse fly ash beads modified with titanium dioxide (TiO<sub>2</sub>), magnesium oxide (MgO), and aluminum oxide (Al<sub>2</sub>O<sub>3</sub>). *Ind. Crop. Prod.* 191, 115928 <https://doi.org/10.1016/j.indcrop.2022.115928>.
- Rahman, N.U., Ullah, I., Alam, S., Khan, M.S., Shah, L.A., Zekker, I., Burlakovs, J., Kallistova, A., Pimenov, N., Vincevica-Gaile, Z., Jani, Y., Zahoor, M., 2021. Activated *Ailanthus altissima* sawdust as adsorbent for removal of acid yellow 29 from wastewater: Kinetics approach. *Water* 13, 2136. <https://doi.org/10.3390/w13152136>.
- Rehman, R., Muhammad, S.J., Arshad, M., 2019. Brilliant green and acid orange 74 dyes removal from water by *Pinus roxburghii* leaves in naturally benign way: an application of green chemistry. *J. Chem.* 2019, 3573704 <https://doi.org/10.1155/2019/3573704>.
- Siddiqui, S.I., Allehyani, E.S., Al-Harbi, S.A., Hasan, Z., Abomuti, M.A., Rajor, H.K., Oh, S., 2023. Investigation of congo red toxicity towards different living organisms: a review. *Processes* 11, 807. <https://doi.org/10.3390/pr11030807>.

- Tejada-Tovar, C., Villabona-Ortíz, A., Ortega-Toro, R., Mancilla-Bonilla, H., Espinoza-León, F., 2021. Potential use of residual sawdust of *Eucalyptus Globulus* Labill in Pb (II) adsorption: Modelling of the kinetics and equilibrium. Appl. Sci. 11, 3125. <https://doi.org/10.3390/app11073125>.
- Temkin, M.I., Pyzhev, V., 1940. Kinetics of ammonia synthesis on promoted iron catalysts. Acta Physicochim. URSS 12, 327–356.
- Tkaczyk, A., Mitrowska, K., Posylniak, A., 2020. Synthetic organic dyes as contaminants of the aquatic environment and their implications for ecosystems: a review. Sci. Total Environ. 717, 137222 <https://doi.org/10.1016/j.scitotenv.2020.137222>.
- Weber, W.J., Morris, J.C., 1963. Kinetics of adsorption carbon from solution. J. Sanit. Eng. Div. 89, 31–60.
- Wekoye, J.N., Wanyonyi, W.C., Wangila, P.T., Tonui, M.K., 2020. Kinetic and equilibrium studies of Congo red dye adsorption on cabbage waste powder. Environ. Chem. Ecotoxicol. 2, 24–31. <https://doi.org/10.1016/j.eneco.2020.01.004>.
- Wong, S., Tumari, H.H., Ngadi, N., Mohamed, N.B., Hassan, O., Mat, R., Saidina Amin, N. A., 2019. Adsorption of anionic dyes on spent tea leaves modified with polyethyleneimine (PEI-STL). J. Clean. Prod. 206, 394–406. <https://doi.org/10.1016/j.jclepro.2018.09.201>.
- Wong, S., Ghafar, N.A., Ngadi, N., Razmi, F.A., Inuwa, I.M., Mat, R., Amin, N.A.S., 2020. Effective removal of anionic textile dyes using adsorbent synthesized from coffee waste. Sci. Rep. 10, 2928. <https://doi.org/10.1038/s41598-020-60021-6>.
- Yang, S., Wang, L., Zhang, X., Yang, W., Song, G., 2015. Enhanced adsorption of Congo red dye by functionalized carbon nanotube/mixed metal oxides nanocomposites derived from layered double hydroxide precursor. Chem. Eng. J. 275, 315–321. <https://doi.org/10.1016/j.cej.2015.04.049>.
- Zhong, C., Feng, B., Zhang, W., Zhang, L., Guo, Y., Wang, T., Wang, H., 2020. The role of sodium alginate in the flotation separation of apatite and dolomite. Powder Technol. 373, 620–626. <https://doi.org/10.1016/j.powtec.2020.07.007>.